数理解析研究所講究録 1400 巻 2004 年 1-20



# Cellular automaton analyses on complex systems – from ants to human beings–

Katsuhiro Nishinari*

*Department of Applied Mathematics and Informatics,*

*Ryukoku University, Shiga 520-2194, Japan.*

Cellular automaton models of complex systems, including vehicular traffic, pedestrian flow and ant trail are presented in this paper. Similarities and differences between these models are discussed by using the fundamental diagram, i.e., the flow-density relation. In the vehicular traffic there exists metastable branches near the critical density. It is shown that the ant model shows an anomalous behaviour due to the existence of pheromone. In appendix, an application of the Painlevé equation is discussed.

## I. INTRODUCTION

Particle-hopping models have been used widely in the recent years to study the spatio-temporal organization in systems of interacting particles driven far from equilibrium [1]. Often such models are formulated in terms of cellular automata (CA) [2]. Examples of such systems include vehicular traffic and pedestrian flow [3–5] where their mutual influence is captured by the inter-particle interactions. Usually, these inter-particle interactions tend to hinder their motions so that the *average speed* decreases *monotonically* with the increasing density of the particles. In a recent letter [6] we have reported a counter-example, motivated by the flux of ants in a trail [7], where, the average speed of the particles varies *non-monotonically* with their density because of the coupling of their dynamics with another dynamical variable.

In this paper, we show cellular automaton models of vehicular traffic, pedestrian flow and ant trail, and discuss similarities and differences between these models by using the fundamental diagram, i.e., the flow-density relation.

*Electronic address: knishi@rins.ryukoku.ac.jp

## II. VEHICLE TRAFFIC MODEL

Recently, cellular automata (CA) have been extensively used for modeling complex phenomena in various fields such as fluid dynamics, statistical physics, biology and other complex systems[1]. Among these CA, the rule-184 CA, which is one of the elementary CA (ECA) proposed by Wolfram[2], has attracted much attention as a model of dynamics of interface[8] and traffic flow[9, 10]. For the model of traffic flow, the rule-184 CA is known to represent the minimal model for movement of vehicles in one lane and show a simple phase transition from free to congested state of traffic flow[3].

In the previous paper[11], by using the ultra-discrete method [12], the Burgers CA(BCA) has been derived from the Burgers equation $\rho_t = 2\rho\rho_x + \rho_{xx}$ which was used by Musha *et al* as a macroscopic traffic model[4][13]. BCA is written as

$$U_j^{t+1} = U_j^t + \min(U_{j-1}^t, L - U_j^t) - \min(U_j^t, L - U_{j+1}^t), \tag{1}$$

where $U_j^t$ denote the number of vehicles at the site $j$ and time $t$. The parameter $L$ represents the maximum capacity of a cell and is related to the lattice interval of the spatial coordinate $x$[11]. Putting the restriction $L = 1$ on (1), BCA is found to be equivalent to the rule-184 CA, which is a prototype of the microscopic traffic models[10]. Since the Burgers equation is considered to be the 1-dimensional Navier-Stokes equation, it is natural to say that (1) is the *Euler representation* of traffic flow. In the Euler description, flow is observed at certain fixed point in space and a dependent variable represents the amplitude of a field at that point. It is noted that the above result has clarified the fact that there is a rigorous the relation between a macroscopic traffic model and a microscopic one in the Euler representation via the ultra-discrete method.

There is the other representation called *Lagrange representation*, which originally also comes from hydrodynamics. In this representation, we observe each particle and follow the trajectory of it. Then we would like to propose the Euler-Lagrange transformation by developing new explicit transformation formulas containing the max and step function, and connect the link of the Euler and Lagrange form in the microscopic models of traffic flow.

First we introduce the variable $u$ by

$$\begin{aligned} S_j^t &= \sum_{k=-\infty}^{j} u_k^t, \\ U_j^t &= u_{Lj+1}^t + u_{Lj+2}^t + \cdots + u_{L(j+1)}^t \\ &= S_{L(j+1)}^t - S_{Lj}^t, \end{aligned} \tag{2}$$

where $u_j^t$ denotes the number of vehicles whose value is zero or one at $j$ th site at time $t$.

Substituting (2) into (1), we obtain

$$S_{Lj}^{t+1} = \max(S_{L(j-1)}^t, S_{L(j+1)}^t - L). \tag{3}$$

Replacing $Lj$ by $j$, this becomes,

$$S_j^{t+1} = \max(S_{j-L}^t, S_{j+L}^t - L). \tag{4}$$

Note that if we put $S_j^t = F_j^t + \frac{j}{2} - \frac{Lt}{2}$, this becomes the ultra discrete diffusion equation,

$$F_j^{t+1} = \max(F_{j-L}^t, F_{j+L}^t). \tag{5}$$

Here, we put

$$S_j^t = \sum_{i=0}^{N-1} H(j - x_i^t), \tag{6}$$

where $H(x)$ is the step function defined by $H(x) = 1$ if $x \geq 0$ and $H(x) = 0$ otherwise, and $N$ is the total number of vehicles on the road. $x_i^t$ is the Lagrange variable that represents the position of the $i$-th car at time $t$ and, of course, the relation $x_0^t < x_1^t < \cdots < x_{N-1}^t$ holds.

By using the newly proposed formula

$$\sum_{k=1}^{n} H(j - \min(a_k, b_k)) = \max\left(\sum_{k=1}^{n} H(j - a_k), \sum_{k=1}^{n} H(j - b_k)\right), \tag{7}$$

where we assume $a_1 < a_2 < \cdots < a_n$ and $b_1 < b_2 < \cdots < b_n$, we obtain the Lagrange form of BCA with general $L$ as

$$x_i^{t+1} = x_i^t + \min(L, x_{i+L}^t - x_i^t - L). \tag{8}$$

The formula (7) expresses the commutability of max function and step function which allows us to manipulate Lagrange variables, and hence it is considered to be a fundamental formula for the Euler-Lagrange transformation.

We should note here that the derived equation (8) is a special case of

$$x_i^{t+1} = x_i^t + \min(V, x_{i+S}^t - x_i^t - S), \tag{9}$$

where $V$ and $S$ are parameters and $V \neq S$ in general. This equation contains the Fukui-Ishibashi model[10] and the quick-to-start model[14] as special cases by putting $S = 1$ and $V = 1$, respectively, thus it is considered as a generalization of these CA models of traffic flow.

Next we will combine the above model with the NS model in order to take into account the randomness of drivers. The NS model is written in Lagrange form as

$$x_i^{t+1} = x_i^t + \max(0, \min(V, x_{i+1}^t - x_i^t - 1, x_i^t - x_i^{t-1} + 1) - \eta_i^t). \tag{10}$$

where $\eta_i^t = 1$ with probability $p$ and $\eta_i^t = 0$ with probability $1 - p$. The last term in the mininum in (10) represents the acceleration of cars. The randomness in this model is considered as a kind of random braking effect, which is known to be responsible for spontaneous jam formation often observed in real traffic [3]. We also consider random accerelation in this model which is not taken into account in the NS model. Thus a stochastic generalization is given in the following set of rules:

1 *Random accerelation*

$$v_i^{(1)} = \min(V_{max}, v_i^{(0)} + \eta_a). \tag{11}$$

where $\eta_a = 1$ with the probability $p_a$ and $\eta_a = 0$ with $1 - p_a$.

2 *Slow-to-start effect*

$$v_i^{(2)} = \min(v_i^{(1)}, x_{i+2}^{t-1} - x_i^{t-1} - 2). \tag{12}$$

3 *Deceleration due to other vehicles*

$$v_i^{(3)} = \min(v_i^{(2)}, x_{i+2}^t - x_i^t - 2). \tag{13}$$

4 *Random braking*

$$v_i^{(4)} = \min(v_i^{(3)} - \eta_b, 0) \tag{14}$$

where $\eta_b = 1$ with the probability $p_b$ and $\eta_b = 0$ with $1 - p_b$.

5 *Avoidance of collision*

$$v_i^{(n+1)} = \min(v_i^{(n)}, x_{i+1}^t - x_i^t - 1 + v_{i+1}^{(n)}) \tag{15}$$

with $n \geq 4$, which is an iterative equation that has to be applied until $v$ converges to $v_i^{(n+1)} = v_i^{(n)} (\equiv v_i)$.

6 *Vehicle movement*

$$x_i^{t+1} = x_i^t + v_i. \tag{16}$$

Again the velocity $v_i$ is used as $v_i^{(0)}$ in the next time step. Step 5 must be applied to each car iteratively until its velocity does not change any more, which ensures that this model is free from collisions. The fundamental diagrams of this stochastic model for some values of $p_a$ and $p_b$ are given in Fig. 1. We see some metastable branches in the fundamental diagram. Moreover, from the spatio-temporal pattern spontaneous jam formation is observed only if we allow random braking. Random accerelation alone is not sufficient to produce spontaneous jamming formation. We also note that a wider scattering area appears if we introduce both random accerelation and braking.

## III. PEDESTRIAN TRAFFIC MODEL

Recent progress in modelling pedestrian dynamics [15] is remarkable and many valuable results are obtained by using different models, such as the social force model [16] and the floor field model [8, 17]. The former model is based on a system of coupled differential equations which has to be solved e.g. by using a molecular dynamics approach similar to the study of granular matter. Pedestrian interactions are modelled via long-ranged repulsive forces. In the latter model two kinds of floor fields, i.e., a static and a dynamic one, are introduced to translate a long-ranged spatial interaction into an attractive local interaction, but with memory, similar to the phenomenon of chemotaxis in biology [18]. It is interesting that, even though these two models employ different rules for pedestrian dynamics, they share many properties including lane formation, oscillations of the direction at bottlenecks [17], and the so-called faster-is-slower effect [16]. Although these are important basics for pedestrian modelling, there are still many things to be done in order to apply the models to more practical situations such as evacuation from a building with complex geometry. In

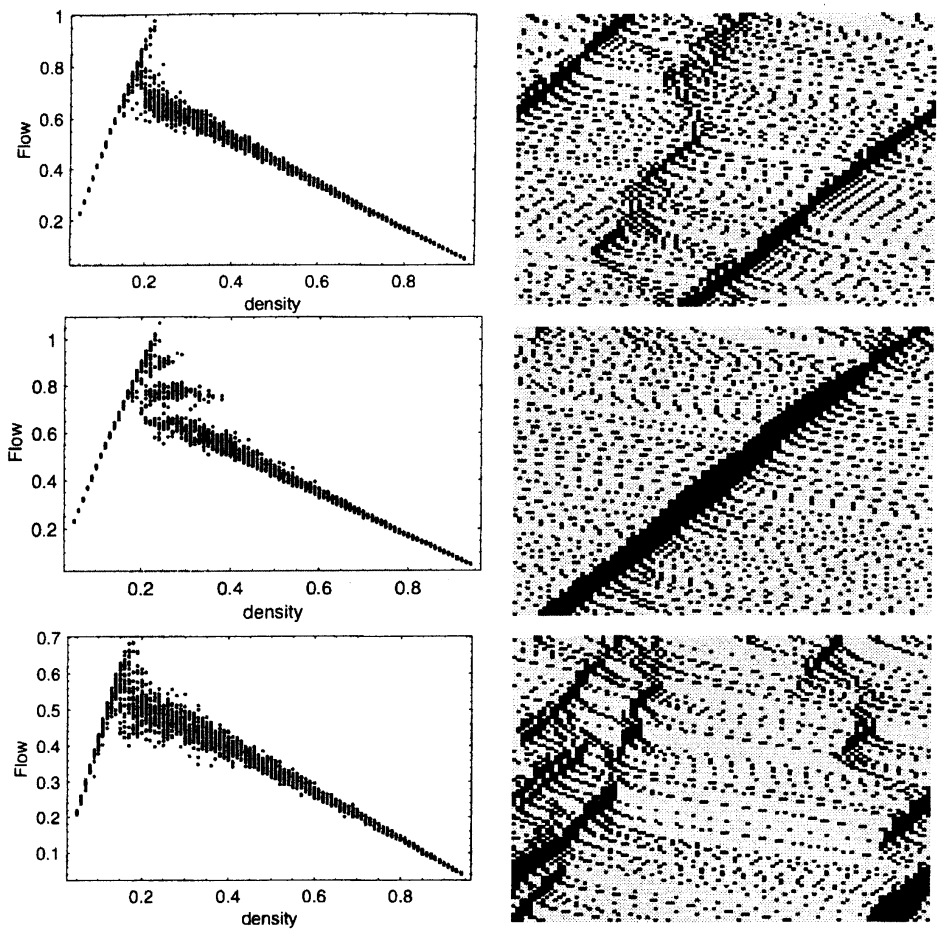


FIG. 1: Fundamental diagrams and typical spatio-temporal patterns of the new stochastic Lagrange model with different value of random parameters. Parameters are set to $V_{max} = 5$ and $S = 2$. Upper two figures are the case of $p_a = 0$ and $p_b = 0.2$, middle ones are $p_a = 0.8$ and $p_b = 0$, and the bottom ones are $p_a = 0.8$ and $p_b = 0.2$.

this paper, we will propose a method to construct the static floor field for complex rooms of *arbitrary* geometry. The static floor field is an important ingredient of the model and has to be specified before the simulations.

First we show the update rules of an extended floor field model for modelling panic behavior of people evacuating from a room. The space is discretized into cells of size 40 cm × 40 cm which can either be empty or occupied by one pedestrian (*hard-core-exclusion*). Each pedestrian can move to one of the unoccupied next-neighbor cells $(i, j)$ (or stay at the present cell) at each discrete time step $t \to t + 1$ according to certain transition probabilities $p_{ij}$ (Fig. 2) as explained below in Sec. III A.

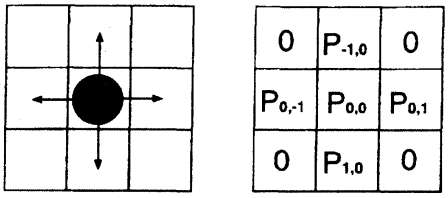


FIG. 2: Target cells for a person at the next time step. The von Neumann neighborhood is used for this model.

For the case of evacuation processes, the *static floor field* $S$ describes the shortest distance to an exit door. The field strength $S_{ij}$ is set inversely proportional to the distance from the door. The *dynamic floor field* $D$ is a *virtual trace* left by the pedestrians similar to the pheromone in chemotaxis [19]. It has its own dynamics, namely diffusion and decay, which leads to broadening, dilution and finally vanishing of the trace. At $t = 0$ for all sites $(i, j)$ of the lattice the dynamic field is zero, i.e., $D_{ij} = 0$. Whenever a particle jumps from site $(i, j)$ to one of the neighboring cells, $D$ at the origin cell is increased by one.

The model is able to reproduce various fundamental phenomena, such as lane formation in a corridor, herding and oscillation at a bottleneck [8, 17]. This is an indispensable property for any reliable model of pedestrian dynamics, especially for discussing safety issues.

### A. Basic update rules

The update rules of our CA have the following structure:

1. The dynamic floor field $D$ is modified according to its diffusion and decay rules, controlled by the parameters $\alpha$ and $\delta$. In each time step of the simulation each single boson of the whole dynamic field $D$ decays with probability $\delta$ and diffuses with probability $\alpha$ to one of its neighboring cells.

2. For each pedestrian, the transition probabilities $p_{ij}$ for a move to an unoccupied neighbor cell $(i, j)$ are determined by the two floor fields and one's inertia (Fig. 2). The values of the fields $D$ (dynamic) and $S$ (static) are weighted with two sensitivity parameters $k_D$ and $k_S$:

$$p_{ij} = N \exp(k_D D_{ij}) \exp(k_S S_{ij}) p_I(i, j) p_W, \tag{17}$$

with the normalization $N$. Here $p_I$ represents the inertia effect [17] given by $p_I(i,j) = \exp(k_I)$ for the direction of one's motion in the previous time step, and $p_I(i,j) = 1$ for other cells, where $k_I$ is the sensitivity parameter. $p_W$ is the wall potential which is explained below. In (17) we do not take into account the obstacle cells (walls etc.) as well as occupied cells.

3. Each pedestrian chooses randomly a target cell based on the transition probabilities $p_{ij}$ determined by (17).

4. Whenever two or more pedestrians attempt to move to the same target cell, the movement of *all* involved particles is denied with probability $\mu \in [0,1]$, i.e. all pedestrians remain at their site [20]. This means that with probability $1-\mu$ one of the individuals moves to the desired cell. Which one is allowed to move is decided using a probabilistic method [17, 20].

5. The pedestrians who are allowed to move perform their motion to the target cell chosen in step 3. $D$ at the origin cell $(i,j)$ of each *moving* particle is increased by one: $D_{ij} \to D_{ij} + 1$, i.e. $D$ can take any non-negative integer value.

The above rules are applied to all pedestrians at the same time (parallel update). Some important details are explained in the following subsections.

### B. Effect of walls

People tend to avoid walking close to walls and obstacles. This can be taken into account by using "wall potentials". We introduce a repulsive potential inversely proportional to the distance from the walls. The effect of the static floor field is then modified by a factor (see eq. (17)):

$$p_W = \exp(k_W \min(D_{\max}, d)), \tag{18}$$

where $d$ is the minimum distance from all the walls, and $k_W$ is a sensitivity parameter. The range of the wall effect is restricted up to the distance $D_{\max}$ from the walls.

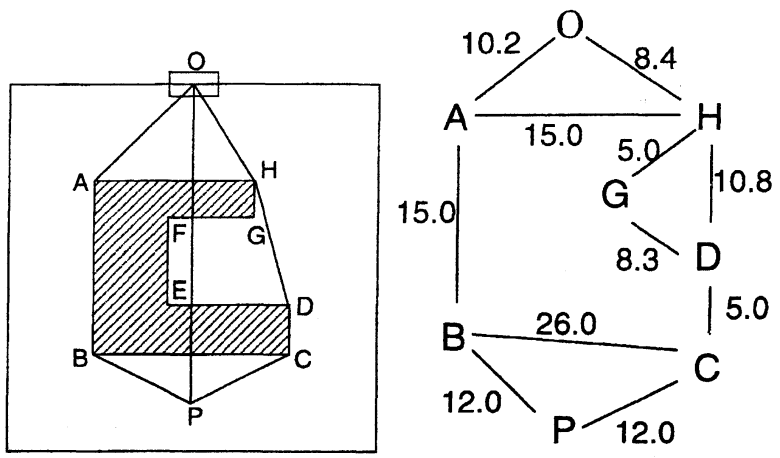


(a) (b)

FIG. 3: Example for the calculation of the static floor field using the Dijkstra method. (a) A room with one obstacle. The door is at $O$ and the obstacle is represented by lines $A - H$. (b) The visibility graph for this room. Each node connected by a bond is "visible", i.e., there are no obstacles between them. The real number on each bond represents the distance between them as an illustration.

### C. Calculation of the static field in arbitrary geometries

In the following we propose a combination of the visibility graph and Dijkstra's algorithm to calculate the static floor field. These methods enable us to determine the minimum Euclidian ($L^2$) distance of any cell to a door with arbitrary obstacles between them.

Let us explain the main idea of this method by using the configuration given in Fig. 3(a) where there is an obstacle in the middle of the room. We will calculate the minimum distance between a cell $P$ and the door $O$ by avoiding the obstacle. If the line $PO$ does not cross the obstacle $A - H$, then the length of the line, of course, gives the minimum. If, however, as in the example given in Fig. 3(a), the line $PO$ crosses the obstacle, one has to make a detour around it. Then we obtain two candidates for the minimum distance, i.e., lines $PBAO$ and $PCDHO$. The shorter one finally gives the minimum distance between $P$ and $O$. If there are more than one obstacle in the room, then we apply the same procedure to each of them repeatedly. Here it is important to note that all the lines pass only the obstacle's edges with an acute angle. It is apparent that the obtuse edges like $E$ and $F$ can never be passed by the minimum lines.

To incorporate this idea into the computer program, we first need the concept of the *visibility graph* in which only the nodes that are visible to each other are bonded [21] ("visible" means here that there are no obstacles between them). The set of nodes consists of a cell point $P$, a door $O$ and all the acute edges in the room. In the case of Fig. 3(a), the node set is $\{P, O, A, B, C, D, G, H\}$ and the bonds are connected between $A - B$, $A - H$, and so on (Fig. 3(b)). Each bond has its own weight which corresponds to the Euclidian distance between them.

Once we have the visibility graph, we can calculate the distance between $P$ and $O$ by tracing and adding the weight of the bonds between them. There are several possible paths between $P$ and $O$, and the one with minimum total weight represents the shortest route between them. The optimization task is easily performed by using the Dijkstra method [21] which enables us to obtain the minimum path on a weighted graph.

Performing this procedure for each cell in the room, the method allows us to determine the static floor field for arbitrary geometries.

### D. Simulations: Inertia effect

We focus on measuring the total evacuation time by changing the parameters $k_S, k_D, k_I, \mu$ and the configuration of the room, such as width, position and number of doors and obstacles. In all simulations we put $D_{\max} = 10$, $\alpha = 0.2$ and $\delta = 0.2$, and von Neumann neighborhoods are used in eq. (17) for simplicity. The size of the room is set to 100 $\times$ 100 cells. Pedestrians try to keep their preferred velocity and direction as long as possible. This is taken into account by adjusting the parameter $k_I$. In Fig. 4, total evacuation times from a room without any obstacles are shown as function of $k_D$ in the cases $k_I = 0$ and $k_I = 3$. We see that it is monotonously increasing in the case $k_I = 0$, because any perturbation from other people becomes large if $k_D$ increases, which causes the deviation from the minimum route. Introduction of inertia effects, however, changes this property qualitatively as seen in Fig. 4. The *minimum* time appears around $k_D = 1$ in the case $k_I = 3$. This is well explained by taking into account the physical meanings of $k_I$ and $k_D$. If $k_I$ becomes large, people become less flexible and all of them try to keep their own minimum route to the exit according to the static floor field regardless of congestion. By increasing $k_D$, one begins to feel the disturbance from other people through the dynamic floor field. This perturbation

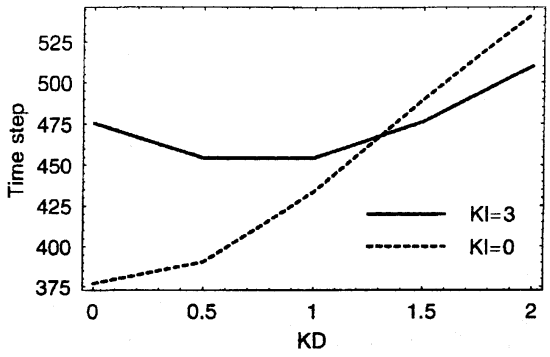


FIG. 4: Total evacuation time versus coupling $k_D$ to the dynamic floor field in the dependence of $k_I$. The room is a simple square without obstacles and 50 simulations are averaged for each data point. Parameters are $\rho = 0.03, k_S = 2, k_W = 0.3$ and $\mu = 0$.

makes one flexible and hence contributes to avoid congestion. Large $k_D$ again works as strong perturbation as in the case of $k_I = 0$, which diverts people from the shortest route largely. Thus we have the minimum time at a certain magnitude of $k_D$, which will depend on the value of $k_S$ and $k_I$.

## IV. ANT TRAIL MODEL

The ants communicate with each other by dropping a chemical (generically called *pheromone*) on the substrate as they crawl forward [19, 22]. Although we cannot smell it, the trail pheromone sticks to the substrate long enough for the other following sniffing ants to pick up its smell and follow the trail. Ant trails may serve different purposes (trunk trails, migratory routes) and may also be used in a different way by different species. Therefore one-way trails are observed as well as trails with counterflow of ants.

In [6] we developed a particle-hopping model, formulated in terms of stochastic CA [2], which may be interpreted as a model of unidirectional flow in an ant-trail. As in ref. [6], rather than addressing the question of the emergence of the ant-trail, we focus attention here on the traffic of ants on a trail which has already been formed. Furthermore we have assumed unidirectional motion. The effects of counterflow, which are important for some species, will be investigated in the future.

Each site of our one-dimensional ant-trail model represents a cell that can accomodate

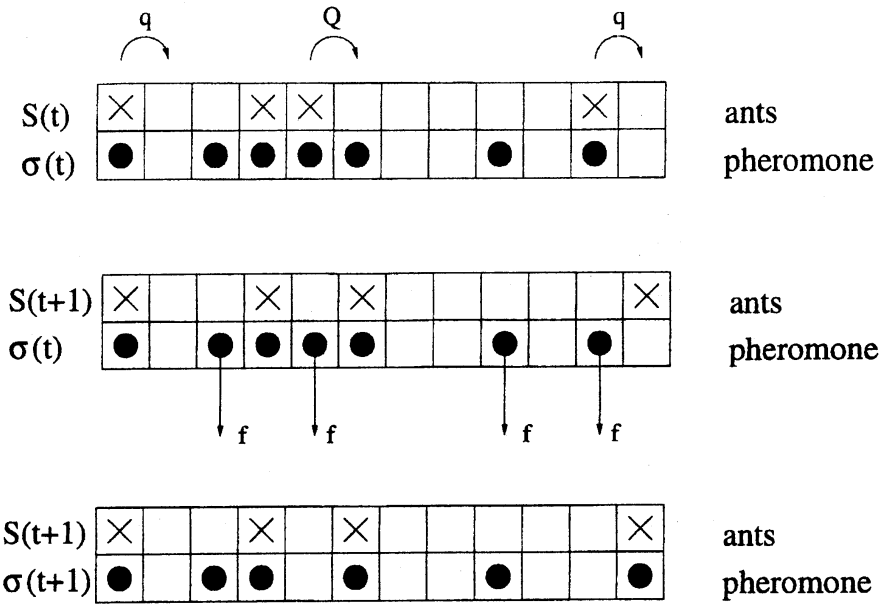


FIG. 5: Schematic representation of typical configurations; it also illustrates the update procedure. Top: Configuration at time $t$, i.e. *before* stage $I$ of the update. The non-vanishing hopping probabilities of the ants are also shown explicitly. Middle: Configuration *after* one possible realisation of *stage* $I$. Two ants have moved compared to the top part of the figure. Also indicated are the pheromones that may evaporate in stage $II$ of the update scheme. Bottom: Configuration *after* one possible realization of *stage* $II$. Two pheromones have evaporated and one pheromone has been created due to the motion of an ant.

at most one ant at a time (see Fig. 5). The lattice sites are labelled by the index $i$ ($i = 1, 2, ..., L$); $L$ being the length of the lattice. We associate two binary variables $S_i$ and $\sigma_i$ with each site $i$ where $S_i$ takes the value 0 or 1 depending on whether the cell is empty or occupied by an ant. Similarly, $\sigma_i = 1$ if the cell $i$ contains pheromone; otherwise, $\sigma_i = 0$. Thus, we have two subsets of dynamical variables in this model, namely, $\{S(t)\} \equiv (S_1(t), S_2(t), ..., S_i(t), ..., S_L(t))$ and $\{\sigma(t)\} \equiv (\sigma_1(t), \sigma_2(t), ..., \sigma_i(t), ..., \sigma_L(t))$. The instantaneous state (i.e., the configuration) of the system at any time is specified completely by the set $(\{S\}, \{\sigma\})$.

Since a unidirectional motion is assumed, ants do not move backward. Their forward-hopping probability is higher if it smells pheromone ahead of it. The state of the system is updated at each time step in *two stages*. In stage I ants are allowed to move. Here the subset $\{S(t+1)\}$ at the time step $t+1$ is obtained using the full information $(\{S(t)\}, \{\sigma(t)\})$ at

time $t$. Stage II corresponds to the evaporation of pheromone. Here only the subset $\{\sigma(t)\}$ is updated so that at the end of stage II the new configuration $(\{S(t+1)\},\{\sigma(t+1)\})$ at time $t+1$ is obtained. In each stage the dynamical rules are applied *in parallel* to all ants and pheromones, respectively.

*Stage I: Motion of ants*

An ant in cell $i$ that has an empty cell in front of it, i.e., $S_i(t)=1$ and $S_{i+1}(t)=0$, hops forward with

$$\text{probability} = \begin{cases} Q & \text{if } \sigma_{i+1}(t)=1, \\ q & \text{if } \sigma_{i+1}(t)=0, \end{cases} \tag{19}$$

where, to be consistent with real ant-trails, we assume $q<Q$.

*Stage II: Evaporation of pheromones*

At each cell $i$ occupied by an ant after stage I a pheromone will be created, i.e.,

$$\sigma_i(t+1)=1 \quad \text{if} \quad S_i(t+1)=1. \tag{20}$$

On the other hand, any 'free' pheromone at a site $i$ not occupied by an ant will evaporate with the probability $f$ per unit time, i.e., if $S_i(t+1)=0$, $\sigma_i(t)=1$, then

$$\sigma_i(t+1) = \begin{cases} 0 & \text{with probability } f, \\ 1 & \text{with probability } 1-f. \end{cases} \tag{21}$$

Note that the dynamics conserves the number $N$ of ants, but not the number of pheromones.

The rules can be written in a compact form as the coupled equations

$$\begin{aligned} S_j(t+1) &= S_j(t) + \min(\eta_{j-1}(t), S_{j-1}(t), 1-S_j(t)) \\ &\quad - \min(\eta_j(t), S_j(t), 1-S_{j+1}(t)), \end{aligned} \tag{22}$$

$$\sigma_j(t+1) = \max(S_j(t+1), \min(\sigma_j(t), \xi_j(t))), \tag{23}$$

where $\xi$ and $\eta$ are stochastic variables defined by $\xi_j(t)=0$ with the probability $f$ and $\xi_j(t)=1$ with $1-f$, and $\eta_j(t)=1$ with the probability $p=q+(Q-q)\sigma_{j+1}(t)$ and $\eta_j(t)=0$ with $1-p$. This representation is useful for the development of approximation schemes.

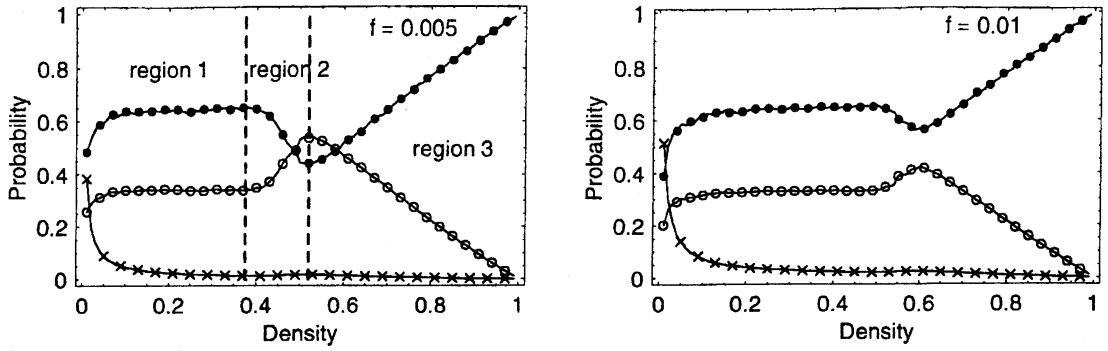


(a) (b)

FIG. 6: Numerical results for the probabilities of finding an ant(•), pheromone but no ant(o) and nothing(×) in front of an ant are plotted against density of the ants. The parameters are $f = 0.005$ (in (a)) and $f = 0.01$ (in (b)).

### A. "Loose" cluster approximation (LCA)

Let us consider again the probabilities $P_a$, $P_p$, $P_0$ defined in the previous section. For the purpose of clarifying some subtle concepts of "clustering" we replot these probabilities for only two specific values of $f$ in Fig. 6; these data have been obtained from computer simulations of our ant-trail model.

There is a flat part of the curves in Fig. 6 in the low density regime; from now onwards, we shall refer to this region as "region 1". Note that in this region, in spite of low density of the ants, the probability of finding an ant in front of another is quite high. This implies the fact that ants tend to form a cluster. On the other hand, cluster-size distribution, obtained from our computer simulations, shows that the probability of finding isolated ants are always higher than that of finding a cluster of ants occupying nearest-neighbor sites[23].

These two apparently contradictory observations can be reconciled by assuming that the ants form "loose" clusters in the region 1. The term "loose" means that there are small gaps in between successive ants in the cluster, and the cluster looks like an usual compact cluster if it is seen from a distance (Fig. 7). In other words, a loose cluster is just a loose assembly of isolated ants. Thus it corresponds to a space region with density larger than the average density $\rho$, but smaller than the maximal density ($\rho = 1$) of a compact cluster.

Let us assume that the loose cluster becomes stationary after sufficient time has passed.

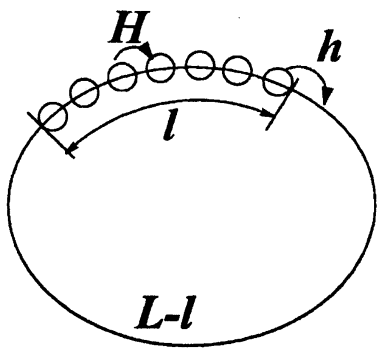


FIG. 7: Schematic explanation of the loose cluster. $H$ is the hopping probability of ants inside the loose cluster and $h$ is that of the leading ant.

Then the hopping probability of all the ants, except the leading one, is assumed to be $H$, while that of the leading one is $h$ (see Fig. 7); the values of $H$ and $h$ are determined self-consistently. Before beginning the detailed analysis, let us consider the properties of $H$ and $h$. If $f$ is small enough, then $H$ will be close to $Q$ because the gap between ants is quite small. On the other hand, if the density of ants is low enough, then $h$ will be very close to $q$ because the pheromone dropped by the leading ant would evaporate when the following ant arrives there.

Next we determine the typical size of the gap between successive ants in the cluster. We will estimate this by considering a simple time evolution beginning with an usual compact cluster (with local density $\rho = 1$) without any gap in between the ants. Then the leading ant will move forward by one site over the time interval $1/h$. This hopping occurs repeatedly and in the interval of the successive hopping, the number of the following ants which will move one step is $H/h$. Thus, in the stationary state, strings (compact clusters) of length $H/h$, separated from each other by one vacant site, will produced repeatedly by the ants (see Fig. 8). Then the average gap between ants is

$$\frac{\left(\frac{H}{h}-1\right)\cdot 0+1\cdot 1}{H/h}=\frac{h}{H}, \tag{24}$$

which is independent of the density $\rho$ of ants. Interestingly, the density-independent average gap in the LCA is consistent with the flat part (i.e., region 1) observed in computer simulations (Fig. 6). In other words, the region 1 is dominated by loose clusters.

Beyond region 1, the effect of pheromone of the last ant becomes dominant. Then the

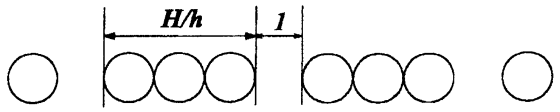


FIG. 8: The stationary loose cluster. The average gap between ants becomes $h/H$, which is irrelevant to the density of ants.

hopping probability of leading ants becomes large and the gap becomes wider, which will increase the flow. We call this region as region 2, in which the "looser" cluster is formed in the stationary state. It can be characterized by a negative gradient of the density dependence of the probability to find an ant in front of a cell occupied by an ant (see Fig. 6).

Considering these facts, we finally obtain the following equations for $h$ and $H$:

$$\left(\frac{h-q}{Q-q}\right)^h = (1-f)^{L-l}, \quad \left(\frac{H-q}{Q-q}\right)^H = (1-f)^{\frac{h}{H}}, \tag{25}$$

where $l$ is the length of the cluster given by

$$l = \rho L + (\rho L - 1)\frac{h}{H}, \tag{26}$$

and $\rho$ and $L$ are density and the system size, respectively. These equations can be applied to the region 1 and 2, and solved simultaneously by the Newton method.

Total flux in this system is then calculated as follows. The effective density $\rho_{\text{eff}}$ in the loose cluster is given by

$$\rho_{\text{eff}} = \frac{1}{1+h/H}. \tag{27}$$

Therefore, considering the fact that there are no ants in the part of the length $L-l$, total flux $F$ is

$$F = \frac{l}{L} f(H, \rho_{\text{eff}}), \tag{28}$$

where $f(H, \rho_{\text{eff}})$ is given by

$$f(H, \rho_{\text{eff}}) = \frac{1}{2}\left(1 - \sqrt{1 - 4H\rho_{\text{eff}}(1-\rho_{\text{eff}})}\right). \tag{29}$$

Above the density 1/2, ants are assumed to be uniformly distributed, in which a kind of MFA works well. We call this region as region 3. Thus we have three typical regions in this model. In region 3, the relation $H = h$ holds because all the gaps have the same length, i.e.

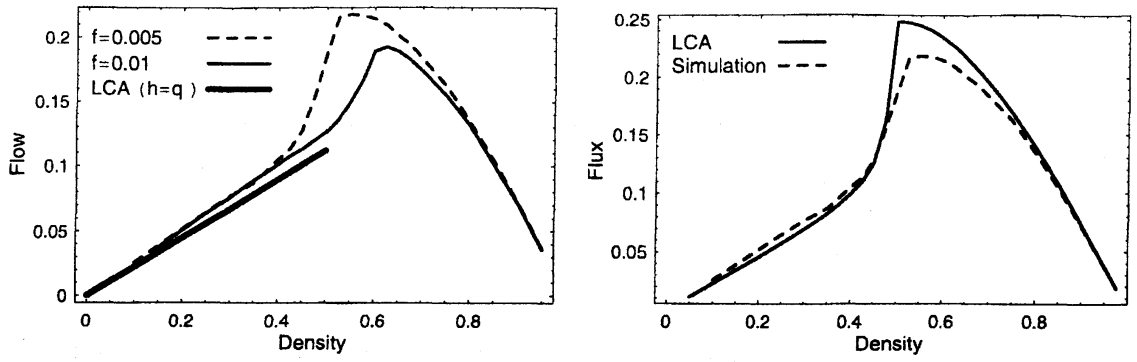


(a) (b)

FIG. 9: (a) Fundamental diagrams of the linear region (bold line) together with numerical results with parameters $f = 0.005$ (broken curve) and $f = 0.01$ (solid curve). (b) The fundamental diagram ($f = 0.005$) of the combination of LCA and (30) (solid curve). The broken curve is the numerical result for $f = 0.005$. The system size is $L = 350$.

the state is homogeneous. Thus $h$ is determined by

$$\left(\frac{h-q}{Q-q}\right)^h = (1-f)^{\frac{1}{\rho}-1}, \tag{30}$$

which is the same as our previous paper, and flux is given by $f(h,\rho)$. It is noted that if we put $\rho = 1/2$ and $H = h$, then (25) coincides with (30).

We can focus on the region 1 by assuming $h = q$ in (25). Under this assumption, we can easily see that the flux-density relation becomes linear. In Fig. 9(a), the two theoretical lines are almost the same, and the gradient of numerical results are also similar among these values of $f$, which is quite similar to the theoretical one. In Fig. 9(b), the results obtained from (25) in the region $\rho \leq 1/2$ are shown. Above this value of density, equation (30) is used. The jointed curve fits quite well the numerical one.

**Acknowledgments**

The author wishes to acknowledge J.Matsukidaira, A.Schadschneider, A.Kirchner and D.Chouwdhury for collaborations of studying CA models presented in this paper.

---

[1] B. Chopard and M. Droz, *Cellular Automata Modeling of Physical Systems* (Cambridge University Press, Australia, 1998).

[2] S. Wolfram, *Theory and applications of cellular automata* (World Scientific, Singapore, 1986).

[3] D. Chowdhury, L. Santen, and A. Schadschneider, Phys. Rep. **329**, 199 (2000).

[4] D. Helbing, Rev. Mod. Phys. **73**, 1067 (2001).

[5] D. Helbing, H. Herrmann, M. Schreckenberg, and D.E.Wolf, *Traffic and Granular Flow '99* (Springer-Verlag, Berlin, 2000).

[6] D. Chowdhury, V. Guttal, K. Nishinari, and A. Schadschneider, J. Phys. A:Math. Gen. **35**, L573 (2002).

[7] M. Burd, D. Archer, N. Aranwela, and D. J. Stradling, American Natur. **159**, 283 (2002).

[8] A. Kirchner and A. Schadschneider, Physica A **312**, 260 (2002).

[9] K. Nagel and M. Schreckenberg, Journal of Physics I France **2**, 2221 (1992).

[10] M. Fukui and Y. Ishibashi, J. Phys. Soc. Jpn. **65**, 1868 (1996).

[11] K. Nishinari and D. Takahashi, J. Phys. A. **31**, 5439 (1998).

[12] T. Tokihiro, D. Takahashi, J. Matsukidaira, and J. Satsuma, Phys. Rev. Lett. **76**, 3247 (1996).

[13] T. Musya and H. Higuchi, J. Phys. Soc. Jpn. **17**, 811 (1978).

[14] K. Nishinari and D. Takahashi, J. Phys. A. **33**, 7709 (2000).

[15] M. Scheckenberg and S. Sharma, *Pedestrian and Evacuation Dynamics* (Springer-Verlag, Berlin, 2001).

[16] D. Helbing, I. Farkas, and T. Vicsek, Nature **407**, 487 (2000).

[17] C. Burstedde, K. Klauck, A. Schadschneider, and J. Zittartz, Physica A **295**, 507 (2001).

[18] E. Ben-Jacob, Contemp. Phys. **38**, 205 (1997).

[19] A. Mikhailov and V. Calenbuhr, *From Cells to Societies* (Springer-Verlag, Berlin, 2002).

[20] A. Kirchner, K. Nishinari, and A. Schadschneider, Phys. Rev. E **67**, 056122 (2003).

[21] M. de Berg, M. van Kreveld, M. Overmars, and O. Schwarzkopf, *Computational geometry*

(Springer-Verlag, Berlin, 1997).

[22] E. Wilson, *The insect societies* (Belknap, Cambridge, USA, 1971).

[23] K. Nishinari, D. Chowdhury, and A. Schadschneider, Phys. Rev. E **67**, 036120 (2003).

## APPENDIX: THE PAINLEVÉ 2 EQUATION AND ITS APPLICATION

In this appendix, application of the Painlevé 2 equation to an engineering process is discussed in order to emphasize the importance of the soliton theory.

Injecting glass fibers in an extruder is an important technology in making plastic materials in order to reinforce them. The injected fibers are, however, sometimes broken into pieces due to inertial forces in the extruder, which damages the strength of materials. Thus it is important to consider under which conditions fibers will break. To this purpose, let us first derive a dynamical equation of a fiber in the extruder. The equation of balance of moments is given by

$$\frac{\partial M}{\partial s} = Q, \tag{A.1}$$

where $M = EI\kappa$ is the moment and $\kappa$ is the curvature of the fiber (Fig.10). $Q$ and $s$ are respectively the shearing force and the arc-length of the fiber. Equations of balance of tangential and transversal force are given by

$$\frac{\partial N}{\partial s} + \kappa Q + q_t = 0 \tag{A.2}$$

$$-\frac{\partial Q}{\partial s} + \kappa N + q_n = 0, \tag{A.3}$$

where $N$ is the normal stress and $q_t, q_n$ are the external force acting on the fiber.

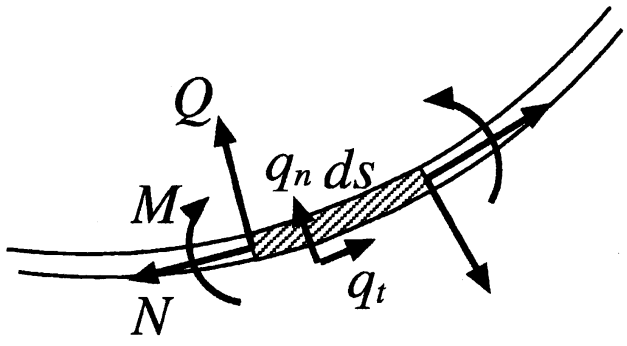


FIG. 10: A segment of a fiber and forces acting on it.

Eliminating $N, Q$ and $M$, we obtain the equation for the curvature as

$$\kappa_{ss} = -\frac{\kappa^3}{2} - \frac{\kappa}{EI}\int q_t ds + \frac{q_n}{EI}. \tag{A.4}$$

In the extruder, it can be shown that we can put both $q_t$ and $q_n$ as a constant. Thus

$$\kappa_{ss} = -\frac{\kappa^3}{2} - C_1 s\kappa + C_2, \tag{A.5}$$

which is nothing but the P2 equation. Boundary conditions are

$$\kappa(0) = \kappa(L) = 0, \tag{A.6}$$

where $L$ is the total length of the fiber, which is usually $\sim$ 10mm. We investigate the P2 equation with the boundary conditions (A.6) numerically. Shooting method is used to adjust the conditions (A.6). A typical result are given in Fig.11. From this figure, we know the maximum curvature of the fiber. If the maximum exceeds the surrender condition of the material, then it will break into pieces and the number of pieces may correspond to the number of extremums appear in the curve.

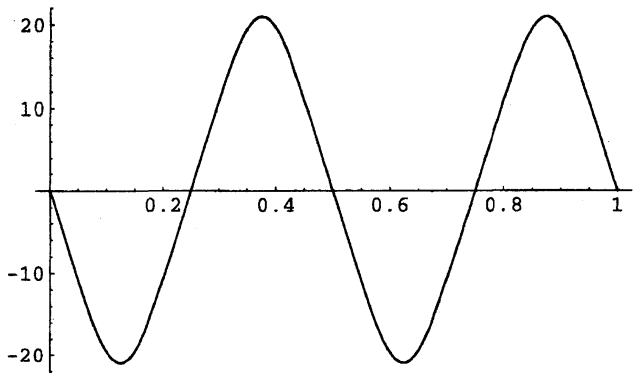


FIG. 11: Numerical results